ELSEVIER

Advances in Colloid and Interface Science 118 (2005) 25 – 42

ADVANCES IN COLLOID AND INTERFACE SCIENCE

www.elsevier.com/locate/cis

Irreversible adsorption of particles on heterogeneous surfaces☆

Zbigniew Adamczyk*, Katarzyna Jaszczółt, Aneta Michna, Barbara Siwek, Lilianna Szyk-Warszyńska, Maria Zembala

Institute of Catalysis and Surface Chemistry, Polish Academy of Sciences, 30-239 Kraków, Niezapominajek 8, Poland

Available online 14 June 2005

Abstract

Methods of theoretical and experimental evaluation of irreversible adsorption of particles, e.g., colloids and globular proteins at heterogeneous surfaces were reviewed. The theoretical models were based on the generalized random sequential adsorption (RSA) approach. Within the scope of these models, localized adsorption of particles occurring as a result of short-ranged attractive interactions with discrete adsorption sites was analyzed. Monte-Carlo type simulations performed according to this model enabled one to determine the initial flux, adsorption kinetics, jamming coverage and the structure of the particle monolayer as a function of the site coverage and the particle/site size ratio, denoted by λ. It was revealed that the initial flux increased significantly with the site coverage Θ_s and the λ parameter. This behavior was quantitatively interpreted in terms of the scaled particle theory. It also was demonstrated that particle adsorption kinetics and the jamming coverage increased significantly, at fixed site coverage, when the λ parameter increased. Practically, for $\alpha=\lambda^2\Theta_s>1$ the jamming coverage at the heterogeneous surfaces attained the value pertinent to continuous surfaces. The results obtained prove unequivocally that spherically shaped sites were more efficient in binding particles in comparison with disk-shaped sites. It also was predicted that for particle size ratio $\lambda<4$ the site multiplicity effect plays a dominant role, affecting significantly the structure of particle monolayers and the jamming coverage. Experimental results validating main aspects of these theoretical predictions also have been reviewed. These results were derived by using monodisperse latex particles adsorbing on substrates produced by covering uniform surface by adsorption sites of a desired size, coverage and surface charge. Particle deposition occurred under diffusion-controlled transport conditions and their coverage was evaluated by direct particle counting using the optical and electron microscopy. Adsorption kinetics was quantitatively interpreted in terms of numerical solutions of the governing diffusion equation with the non-linear boundary condition derived from Monte-Carlo simulations. It was proven that for site coverage as low as a few percent the initial flux at heterogeneous surfaces attained the maximum value pertinent to homogeneous surfaces. It also was demonstrated that the structure of larger particle monolayers, characterized in terms of the pair correlation function, showed much more short-range ordering than predicted for homogeneous surface monolayers at the same coverage. The last part of this review was devoted to detection of polyelectrolyte multilayers on various substrates via particle deposition experiments.

Keywords: Adsorption of colloids; Colloid adsorption; Heterogeneous surface adsorption; Irreversible adsorption; Kinetics of particle adsorption; Protein adsorption; Random site adsorption

Contents

1. Introduction . . . 26
2. Theoretical models . . . 26
3. Illustrative experimental results . . . 32
4. Conclusions . . . 40
Acknowledgments . . . 41
References . . . 41

☆ This work was presented at the "Non-equilibrium Colloidal Phenomena 2004" Conference, Cracow, Poland.

* Corresponding author.
E-mail address: ncadamcz@cyf-kr.edu.pl (Z. Adamczyk).

0001-8686/$ - see front matter © 2005 Elsevier B.V. All rights reserved.
doi:10.1016/j.cis.2005.03.003

1. Introduction

Adsorption and deposition (irreversible adsorption) of colloids, proteins and other bio-materials on solid/liquid interfaces is of large significance for many practical and natural processes such as filtration, paper-making, chromatography, separation of proteins, viruses, bacteria, pathological cells, immunological assays, thrombosis, biofouling, biomineralisation, etc. The effectiveness of these processes is often enhanced by the use of coupling agents bound to interfaces (called often precursor films), e.g., polyelectrolytes [1–8]. By using the alternative layer-by-layer deposition method involving polyelectrolytes, multilayer particle films of a targeted architecture can be produced [9–13]. In biomedical applications special proteins (antibodies) attached to the surface are used for a selective binding of a desired ligands from protein mixtures as is the case of the affinity chromatography [14], recognition processes (biosensors) [15,16], immunological assays [17,18], etc.

On the other hand, many of experimental studies on colloid particle adsorption have been carried out for surfaces modified by adsorption of surfactants, polyvalent ions, or chemical coupling agents (silanes), which change the natural surface charge of substrate surfaces [19,20]. Another important example is adsorption of ionic species, e.g., heavy metal ions, at oxide surfaces bearing various sites, usually characterized by a wide spectrum of binding energy [21]. This often leads to nonuniform distribution of charge as is the case for packed bed filtration procedures [22,23]. Appearance of such heterogeneous interfaces may exert important influence on transport and distribution of colloid contaminants in aqueous porous media, e.g., in soils [24].

A characteristic feature of all these processes, also comprising chemisorption of gases on solids, is that the solute (ion, particle or protein) adsorption occurs at heterogeneous surfaces bearing isolated adsorption sites.

Therefore, the goal of this paper is to review selected methods of theoretical and experimental evaluation of irreversible adsorption of particles, e.g., colloids and globular proteins at heterogeneous surfaces. These theoretical approaches are based on the generalized random sequential adsorption (RSA) model whereas experiments concern colloid adsorption on substrates produced by covering uniform surfaces by adsorption sites of a desired size, coverage and surface charge. A part of this review is devoted to the interesting problem of detection of polyelectrolyte multilayers on various substrates via particle deposition experiments.

2. Theoretical models

A theoretical modeling of irreversible adsorption of particles on surfaces exhibiting a continuous distribution of adsorption sites has extensively been carried out in terms of the random sequential adsorption (RSA) model [25–35]. The number of sites in these simulations was considerably larger than the number of adsorbed particles (practically infinite) and their dimensions were negligible in comparison with particle dimensions.

In order to deal with a more realistic situation of a discrete distribution of sites, Jin et al. [36,37] developed a more general RSA approach, referred to as the random site surfaces model (RSS). In this model the sites (surface heterogeneities) of a finite number were assumed to be in the point-like form. A correspondence (mapping function) between the adsorption process at the RSS surfaces and the widely studied continuous surface RSA model was found.

Later on, more elaborate models have been developed considering finite dimensions of sites having the form of either hard discs of the diameter $2a_s$ incorporated into the substrate [38], see Fig. 1, part (a) or hard spheres attached to the surface [39,40], see Fig. 1, part (b). The configuration of the sites can be produced in a number of ways, e.g., by quenching an equilibrium fluid of a given coverage, or by performing the continuous RSA simulations that is the usual procedure adopted in these works [38–40]. Adsorption kinetics, particle configurations and the jamming coverage were determined via Monte-Carlo type simulations as a function of the particle/site size ratio $\lambda = a_p/a_s$ (where $2a_p$ is the adsorbing particle diameter) and site coverage Θ_s. It should be mentioned, however, that the range of applicability of the disk model is limited by the fact that such a site configuration is rather specific and difficult to realize in practice.

A more relevant for practical applications seems the sphere-shaped adsorption site model. The basic assumption of this model is that the colloid particle (of a spherical shape) can only be adsorbed upon touching the site, see Fig. 1, part “b”. Otherwise, at bare interface, the particle will not adsorb. Physically, this corresponds to the situation when the particles are irreversibly bound to the sites due to short-ranged attractive interactions of an electrostatic or chemical nature. Furthermore, particle adsorption was assumed irreversible and localized, which means that all particle positions remained fixed during the entire simulation run.

As mentioned, the surfaces were precovered by sites according to the classical RSA model pertinent to continuous surfaces [38–40]. The number of spherically shaped sites was N_s^o distributed over a homogeneous surface having the geometrical surface area ΔS (without loss of generality one can assume $\Delta S = 1$ and normalize accordingly the sphere dimension). The surface concentration (2D density) of the sites is then equal to N_s^o and the dimensionless coverage is defined as $\Theta_s = \pi a_s^2 N_s^o$. As proved in previous numerical simulations [27–29] the distribution of sites generated in the RSA processes for $\Theta_s < 0.1$ remains quasi-random. For higher coverage, however, the distribution of sites becomes correlated since the number of pairs at closer separations is larger than the average. This can be quantitatively characterized in terms of the pair correlation function as discussed in Refs. [26–34].

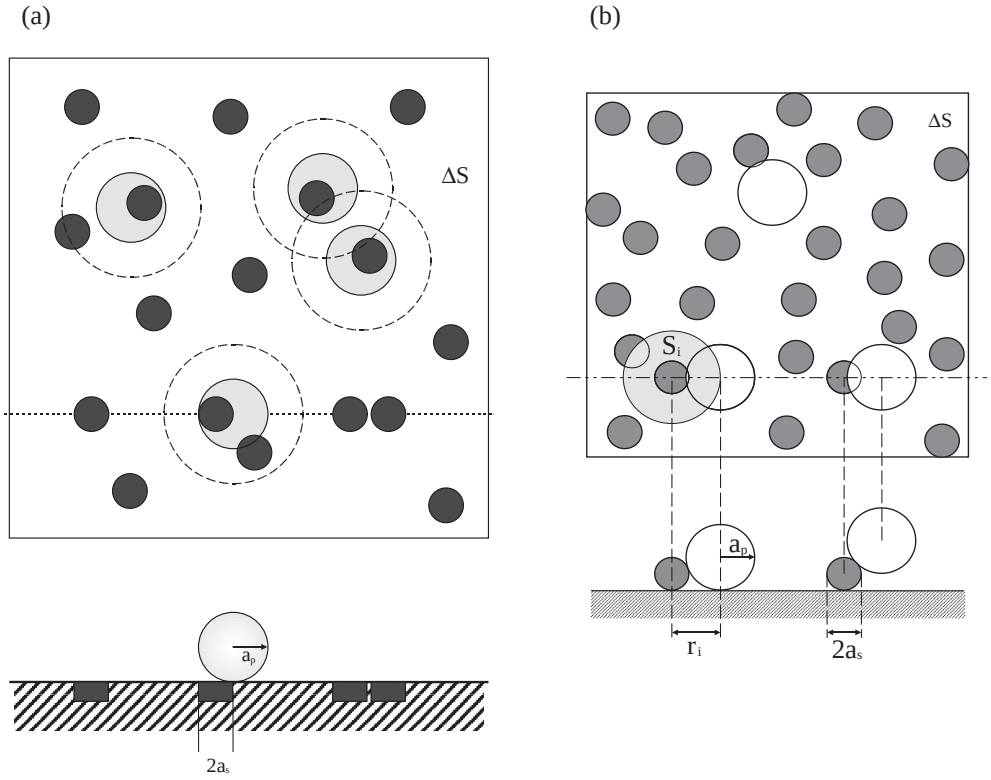

Fig. 1. Part (a): A schematic view of particle adsorption at heterogeneous surfaces bearing disk-shaped adsorption sites. Part (b): Same as for part (a) but for spherically shaped adsorption sites. From Refs. [38,39].

The consecutive adsorption of particles at the surface covered by sites was simulated according to the algorithm [38,39]:

(i) an adsorbing (virtual) particle of the diameter $2a_p$ was generated at random within the simulation area, if it did not touch any of sites, the particle was rejected and another virtual particle was produced (the number of attempts N_{att} was increased by 1),
(ii) otherwise, if the particle touched any of the sites, the overlapping test was performed according to the usual RSA rules, i.e., it was checked if there is any previously adsorbed particle within the exclusion volume (see Fig. 1b); if there was overlapping the simulation loop was repeated (the number of attempts was increased by 1),
(iii) if there was no overlapping the virtual particle was assumed irreversibly adsorbed at the given position and its coordinates were stored, the number of adsorbed particles N_p is increased by 1.

It should be mentioned that particle adsorption at heterogeneous surfaces modeled by spherically shaped sites is a truly three-dimensional process, oppositely to adsorption at disk-shaped sites [38] or adsorption at precovered surfaces considered in [41,42]. In the latter case particle adsorption occurred at a free substrate surface devoted of preadsorbed particles (sites). This situation corresponds to the case when there is repulsion between adsorbing particles and sites and attraction between particles and the substrate surface.

Similarly as in classical RSA simulation, adsorbed particle coverage at heterogeneous surfaces was calculated as $\Theta_p = \pi a_p^2 N_p$. Accordingly, the dimensionless adsorption time is defined as [38–40]

$$\tau = \pi a_p^2 \frac{N_{att}}{\Delta S} = \pi a_p^2 N_{att} \quad (1)$$

This definition allowed one to derive kinetics of particle adsorption, i.e., the dependence of Θ_p vs. the adsorption time τ.

An alternative evaluation of particle adsorption kinetics can be achieved via the available surface function (ASF) approach introduced in [25,27] and extended to heterogeneous surfaces in [38–40]. This function can be defined as normalized probability p of adsorbing a particle for a fixed coverage and configuration of sites and particles knowing their configuration. Additionally, the ASF is dependent on the particle to site size ratio λ. This function can effectively be evaluated from the above simulation scheme by performing, at fixed Θ_s, Θ_p, a large number of adsorption trials N_{att}, N_{succ} of them being potentially successful. Then, the ASF is defined as the limit of N_{succ}/N_{att} when $N_{att} \to \infty$. Especially important is the value of ASF in the limit of negligible particle coverage, $\Theta_p \to 0$ since it characterizes the initial flux to heterogeneous surfaces. This quantity is of

a primary interest from experimental viewpoint. Knowing ASF one can calculate particle adsorption kinetics by integrating the constitutive dependence [27–29].

$$\frac{d\Theta_p}{d\tau} = p \tag{2}$$

As discussed in Refs. [43,44] this classical concept of the ASF may be not general enough to deal with the diffusion-controlled adsorption of particles. More refined approaches, considering various transport mechanisms of particles in the bulk, have been proposed [31,45]. However, due to insurmountable mathematical problems, their applicability for heterogeneous surface adsorption seems prohibitive. Therefore, the standard ASF concept seems appropriate since it reflects the most important features of the problem of particle adsorption at heterogeneous surfaces. This function also can be used for specifying boundary conditions for the bulk transport equation as shown in [46–48].

On the other hand, the structure of particle monolayer produced in the above RSA process can be quantitatively characterized in terms of the pair correlation function $g(r)$ (often referred to the radial distribution function RDF), defined as [28,29]

$$g(r) = \frac{\pi a_p^2}{\Theta_p}\left\langle \frac{\Delta N_p}{2\pi r \Delta r}\right\rangle \tag{3}$$

where $\langle\ \rangle$ means the ensemble average and N_p is the number of particles adsorbed within the ring $2\pi r\Delta r$ drawn around a central particle. The function can be interpreted as an averaged probability of finding a particle at the distance r from another particle (with the center located at $r=0$) normalized to the uniform probability at large distances. For sake of convenience the distance r is usually normalized by using the particle radius a_p as a scaling variable.

It is to mention that the distance r was measured between the projection of the adsorbed particle centers on the adsorption plane. Obviously, all particles located close to the perimeter of the simulation area were discarded from the averaging procedure. In order to obtain a satisfactory accuracy of $g(r)$, particle populations reaching 10^5 are usually considered [38,39].

It is interesting to observe that despite the complexity of the problem of particle adsorption at heterogeneous surfaces, some useful analytical expressions were derived for low coverage of adsorbed particles. These expressions having a practical significance can be exploited for testing the validity of numerical simulations.

From simple geometrical considerations one can deduce that the particle adsorbs if the distance between its center projected on the adsorption plane and the site center r_i becomes smaller than $2\sqrt{a_p a_s}$ (see Fig. 1b). Hence the interaction area of the particle with the site is

$$S_i = \pi r_i^2 = 4\pi a_p a_s \tag{4}$$

If the site distribution can be treated as uniform, the probability of finding any site within the interaction area can be calculated from the Poisson distribution as

$$p_0 = 1 - e^{-S_i N_s^0} = 1 - e^{-4\lambda\Theta_s} \tag{5}$$

This probability, which can be identified with the ASF, describes the initial flux of particles when $\Theta_p \to 0$.

Obviously, Eq. (5) becomes less accurate in the limit of larger Θ_s when the distribution of the sites deviates from an uniform distribution [27]. A more accurate expression can be formulated by exploiting the results discussed in [41]. By exploiting the scaled particle theory of Reiss et al. [49] it was demonstrated that the probability of finding a cavity of surface area S_i devoted of sites (smaller-sized particles) is given by the formula

$$p_c = B_p^0 = (1-\Theta_s)e^{-\frac{(4\lambda-1)\Theta_s}{1-\Theta_s} - \left[\frac{(2\sqrt{\lambda}-1)\Theta_s}{1-\Theta_s}\right]^2} \tag{6}$$

where B_p^0 is defined as the surface blocking function for the analogous problem of particle adsorption over surfaces precovered with smaller-sized particles (when adsorption occurs at the uncovered interface only). Since the probability of finding a site within the interaction area equals $1-p_c$ one can predict that [39]

$$p_0 = 1 - B_p^0 = 1 - (1-\Theta_s)e^{-\frac{(4\lambda-1)\Theta_s}{1-\Theta_s} - \left[\frac{(2\sqrt{\lambda}-1)\Theta_s}{1-\Theta_s}\right]^2} \tag{7}$$

In the limit of initial adsorption stage, when particle coverage Θ_p remains small and the site coverage fulfills the inequality $\Theta_s < 1/4\lambda$, one can approximate the ASF function of particles by the Langmuir-like formula [39]

$$\begin{aligned} p &= 4\lambda\Theta_s(1-\Theta_p/\lambda^2\Theta_s n_s)(1-q\Theta_p) \\ &\cong p_0(1-\Theta_p/\Theta_p^{mx}) \end{aligned} \tag{8}$$

where n_s is the site coordination number (multiplicity) to be determined from numerical simulations and the multiplier $(1-q\Theta_p)$ accounts for exclusion effects among particles (lowest order correction), q is the dimensionless exclusion area equal 4 in the case of hard spheres, and $\Theta_p^{mx} = \lambda^2 n_s\Theta/(1+q\lambda^2 n_s\Theta_s)$. From simple geometry one can deduce that for $\lambda > 4$ one site can coordinate only one particle, so $n_s = 1$.

For $\Theta_p \to 0$, Eq. (8) reduces to the simple expression describing the initial adsorption probability of particles on surfaces sparely covered by sites

$$p_0 = p = 4\lambda\Theta_s \tag{9}$$

It is interesting to mention that for disc-shaped sites the initial adsorption probability $p_0 = \Theta_s$.

The p_0 function is of a primary practical interest because it represents the averaged probability of adsorbing the particle at surfaces covered by a given number of sites. Hence, by knowing p_0 one can calculate the initial flux of solute (particles) to heterogeneous surfaces. The dependence of p_0 on Θ_s calculated for $\lambda = 2$, 5 and 10 [39] is plotted in Fig. 2. As can be noticed the adsorption probability of particles increases abruptly with Θ_s, especially for larger λ

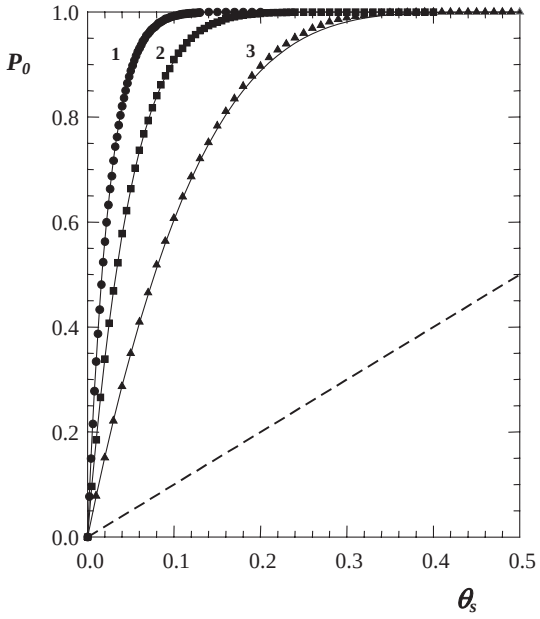

Fig. 2. The dependence of the initial adsorption probability p_0 on surface coverage of adsorption sites Θ_s; the points denote numerical simulations performed for (1) $\lambda=10$, (2) $\lambda=5$ and (3) $\lambda=2$. The solid lines represent the analytical results derived from Eq. (7) and the dashed line shows the analytical predictions for adsorption on disk-shaped sites, when $p_0=\Theta_s$. From Ref. [39].

values. For $\lambda=10$, the probability of adsorption reaches unity (the value pertinent to homogeneous surfaces) for Θ_s as low as 0.1. This behavior is well reflected by Eq. (7) being in a quantitative agreement with the numerical data for the entire range of Θ_s and λ studied. It is also interesting to note that adsorption probability at spherical sites becomes considerably larger than for disc-shaped sites (see the dashed line in Fig. 2). This observation has practical implications showing that the geometry of the active sites plays a more decisive role than their surface concentration. The results shown in Fig. 2 further imply that by measuring experimentally the flux of larger colloid particles (which can easily be done by direct microscope observations) one can detect the presence of nano-scale surface heterogeneities, invisible under the microscope. If the surface concentration of the sites can be estimated one can determine their size or shape from the particle deposition experiments.

One should remember, however, that the results shown in Fig. 2 describe particle adsorption rate at heterogeneous surfaces in the limit when their accumulation is negligible, i.e., for $\Theta_p\to 0$ only. If Θ_p becomes finite, the probability of particle adsorption decreases as a result of volume exclusion effects (often referred to less accurately as the surface blocking effects). The adsorption probability (ASF) is then a function of Θ_s, Θ_p and λ as analyzed extensively in Ref. [39].

It was shown that in the case when $\alpha=\lambda^2\Theta_s>1$ particle adsorption at heterogeneous surfaces can be approximated by the function

$$p = p_0 B\left(\Theta_p\right) \tag{10}$$

where the $p_0(\lambda,\Theta_s)$ function is given by Eq. (7) and $B(\Theta_p)$ can be calculated from various analytical fitting functions having of the type [27,33,34]

$$B\left(\overline{\Theta}_p\right) = f\left(\overline{\Theta}_p\right)\left(1-\overline{\Theta}_p\right)^3 \tag{11}$$

where $\overline{\Theta}_p=\Theta_p/\Theta_p^\infty$, Θ_p^∞ is the jamming coverage and $f(\overline{\Theta}_p)$ are low-order polynomials. One of the most accurate expressions for $f(\overline{\Theta}_p)$ has the form [27]

$$f\left(\overline{\Theta}_p\right) = 1 + 0.812\overline{\Theta}_p + 0.426\overline{\Theta}_p^2 + 0.0716\overline{\Theta}_p^3 \tag{12}$$

As can be deduced from Eqs. (11) and (12), in the limit when $\overline{\Theta}_p\to 1$ the blocking function assumes the form

$$B\left(\overline{\Theta}_p\right) \cong 2.32\left(1-\overline{\Theta}_p\right)^3 \tag{13}$$

These results have significance because all results known previously for homogeneous surfaces can directly be transferred to heterogeneous surface adsorption. In particular, by substituting the expression for the ASF given by Eq. (10) into the constitutive dependence, Eq. (2) one obtains

$$\int_0^{\overline{\Theta}_p} \frac{d\overline{\Theta}'}{B(\overline{\Theta}')} = p_0\tau/\Theta_p^\infty = \tau' \tag{14}$$

One can deduce from Eq. (14) that all the kinetic results known previously for the continuous surfaces can be directly transferred to heterogeneous surfaces by introducing the transformed adsorption time $\tau'=p_0(\Theta_s,\lambda)/\Theta_p^\infty$. In particular, by substituting Eq. (13) into Eq. (14) one obtains upon integration the limiting result

$$\Theta_p(\tau) = \Theta_p^\infty\left(1-\frac{C}{\sqrt{\tau'}}\right) \tag{15}$$

where

$$C = \sqrt{\frac{\Theta_p^\infty}{4.64 p_0}} \tag{16}$$

However, in the general case, with $B(\overline{\Theta}_p)$ given by Eq. (11), the integration procedure is rather awkward.

Rather than discuss further the kinetic aspects of particle adsorption at heterogeneous surfaces we concentrate on the jamming coverage Θ_p^∞ that has a major practical significance. Extensive simulations performed in Refs [39,40] enabled one to determine this as a function of Θ_s and λ. The results plotted as Θ_p^∞ vs. Θ_s (in logarithmic scale) are collected in Fig. 3 (solid lines). The limiting analytical results predicted for low site coverage, i.e., $\Theta_p^\infty=\lambda^2\Theta_s n_s$ also are plotted for comparison (dashed lines in Fig. 3). It was demonstrated in Ref. [39] that for $\lambda>2$ the numerical results can well be interpolated by the simple analytical function

$$\Theta_p^\infty = \Theta_\infty\left(1-e^{-\frac{\lambda^2\Theta_s}{\Theta_\infty}}\right) \tag{17}$$

where $\Theta_\infty=0.547$ is the jamming coverage for uniform surfaces.

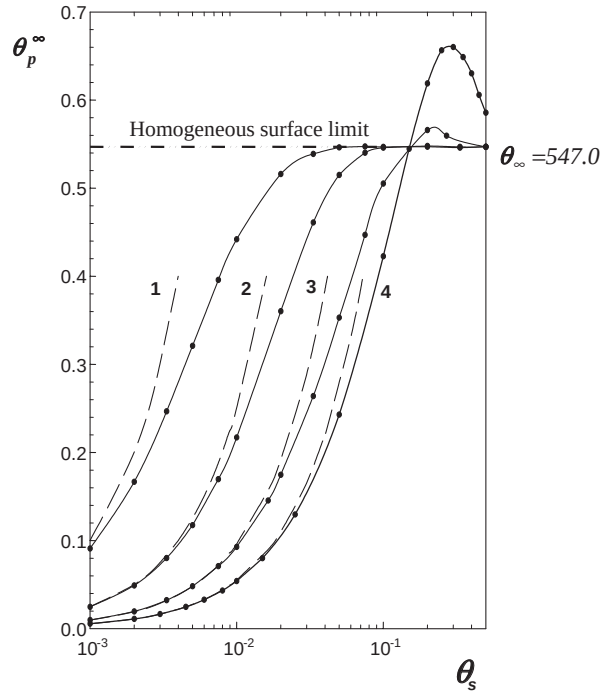

Fig. 3. The dependence of the jamming coverage of particles Θ_p^∞ on the coverage of the spherically shaped adsorption sites Θ_s; the points denote the results of numerical simulations, performed for (1) $\lambda=10$, (2) $\lambda=5$, (3) $\lambda=2$ and (4) $\lambda=1$. The solid lines represent the results calculated from the fitting function given by Eq. (17) (for $\lambda>2$) and the dashed lines show the results derived from the Langmuir model, i.e., $\Theta_p=\lambda^2\Theta_s n_s$.

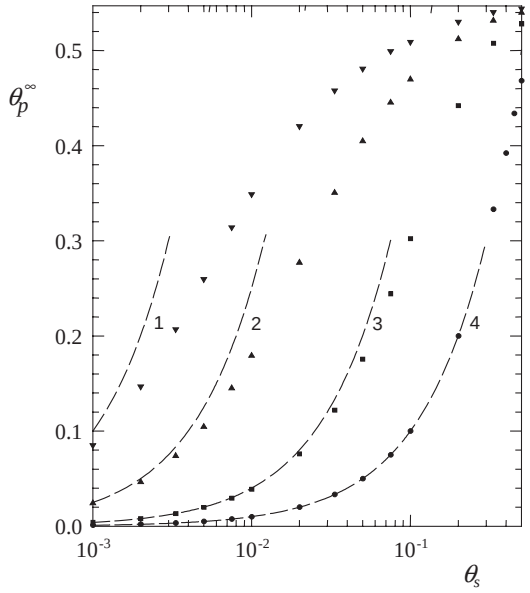

Fig. 4. The dependence of the jamming coverage of particles Θ_p^∞ on the coverage of the disc-shaped adsorption sites Θ_s; the points denote the results of numerical simulations, performed for (1) $\lambda=10$, (2) $\lambda=5$ and (3) $\lambda=2$ (4) $\lambda=1$. The dashed lines show the results derived from the Langmuir model, i.e., $\Theta_p=\lambda^2\Theta_s$. From Ref. [38].

This formula gives a satisfactory accuracy for the entire range of Θ_s studied. However, it breaks down for $\lambda=2$ and 1 when a maximum on the Θ_p vs. Θ_s dependence is observed for Θ_s about 0.25. This maximum jamming coverage for $\lambda=2$ attained the value of 0.57, being slightly larger than for adsorption at uniform surfaces when the jamming coverage was 0.547 [26]. The maximum appears because, for Θ_s about 0.2–0.3, the area accessible for adsorption becomes larger than the geometrical interface area because particles can touch the sites at various distances from the interface. When Θ_s increases further above this critical value, the accessible area becomes again very close to the geometrical interface area. Although this effect is interesting from a theoretical point of view it does not to have significant experimental implications. This is so because in practice it is very difficult to measure surface coverage of particles with a relative accuracy better than 5% due to the polydispersity of real particle suspensions [30]. This hypothesis is confirmed by the fact that in the case of disc-shaped sites, when all particles are adsorbed at the interface area covered by sites (in one plane), no such maximum appears (see Fig. 4). Because of the 3D adsorption the jamming coverage in the case of spherical adsorption sites increases with Θ_s more abruptly than for disc-shaped sites.

The deviation from Eq. (17) for $\lambda=2$ and 1 also appears for low site coverage. It was demonstrated in Refs. [39,48] that this is caused by multiple site coordination meaning physically that more than one particle can be attached simultaneously to one adsorption site. This effect is better illustrated in Fig. 5 where the dependence of Θ_p^∞ on site coverage the parameter $\lambda^2\Theta_s$ is plotted. The slope of this

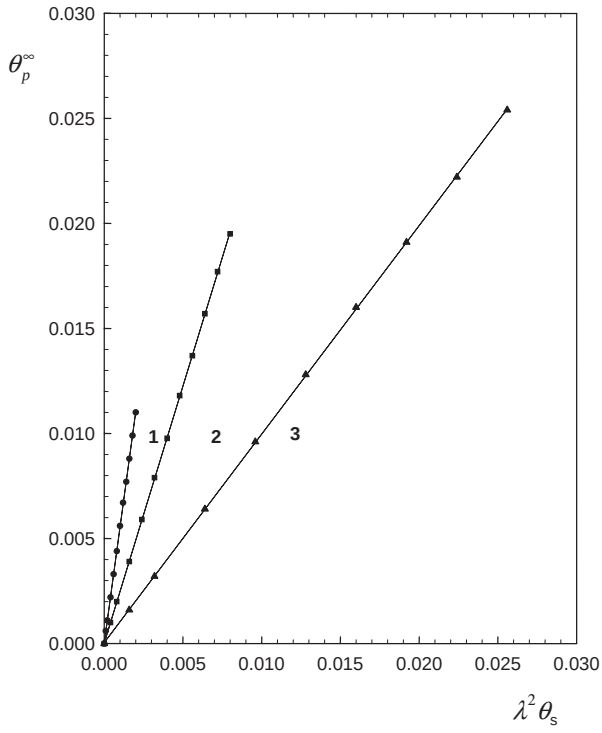

Fig. 5. The dependence of the jamming coverage of particles Θ_p^∞ on the $\lambda^2\Theta_s$ parameter; the points denote the results of numerical simulations, performed for (1) $\lambda=1$, (2) $\lambda=2$ and (3) $\lambda=5$. The solid lines represent the linear regression.

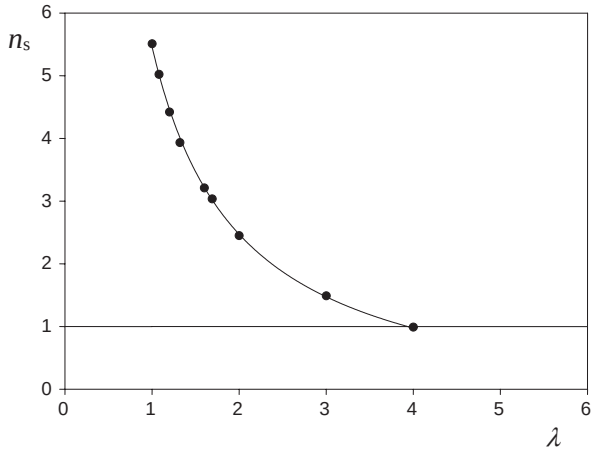

Fig. 6. The dependence of the site coordination number n_s on λ (particle to site size ratio). The solid line represents the hyperbolic fitting function $n_s = -0.5168 + 5.967/\lambda$.

dependence in the limit of Θ_s tending to zero gives directly the site coordination number n_s. One can see that for $\lambda = 5$ the site coordination equals 1, which can be easily deduced from simple geometry. For $\lambda = 2$, $n_s = 2.4$ and $\lambda = 1$, $n_s = 5.5$.

The theoretical dependence of n_s on λ is plotted in Fig. 6. It can well be fitted by the simple interpolating function

$$n_s = 5.967/\lambda - 0.517 \quad (18)$$

One can notice in Fig. 6 that n_s increases abruptly when the size of the particle approaches the site dimension. Results shown in Fig. 6 also suggest that particle clusters of targeted composition, i.e., containing between two and six particles coordinated at one site, can be produced by exploiting the particle deposition process.

This is spectacularly illustrated in Fig. 7 where a series of particle monolayers pictures is plotted for $\Theta_s = 0.03$ and the increasing coverage of particles.

By exploiting these findings one can deduce that for not too large Θ_s, the jamming coverage of particles is given by

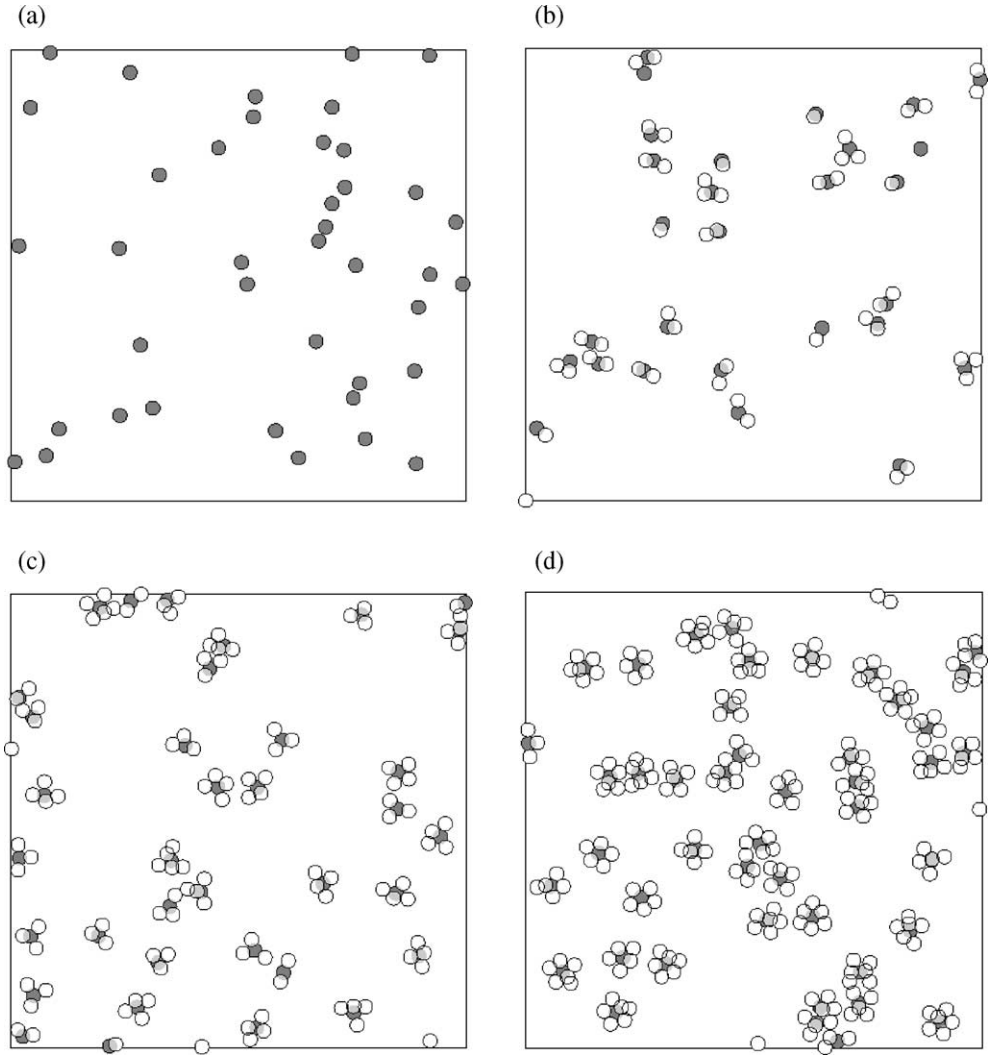

Fig. 7. Monolayers of particles adsorbed at heterogeneous interfaces covered by sites derived from numerical simulations ($\lambda = 1$, $\Theta_s = 0.03$). (a): $\Theta_p = 0$; (b): $\Theta_p = 0.05$; (c): $\Theta_p = 0.1$; (d): $\Theta_p = 0.15$.

the expression $\Theta_p^{\infty}=n_s\lambda^2\Theta_p$, with n_s calculated from Eq. (18). Once Θ_p^{∞} is known one can unequivocally evaluate the blocking function $B(\Theta_p)$ via Eq. (11) and particle adsorption kinetics via Eq. (14) or its integrated form, Eq. (16). As discussed in some detail elsewhere [31,32,35,46] such an approach is valid when the thickness of the diffusion boundary layer remains comparable with adsorbing particle dimension. This requirement is fulfilled for micrometer-sized particles under forced convection transport conditions only [32]. For smaller particles and the diffusion-controlled transport conditions the coupling between the bulk and surface transport should be considered via the approach developed in [31,32,46] for uniform surfaces. According to this model, Eq. (10) can be exploited as the boundary condition for the bulk transport problems. In this way the main features of particle adsorption at heterogeneous surface can be properly reflected, in particular the initial adsorption rate and the jamming coverage. However, due to complicated topology, a more detailed description of these processes requires further theoretical studies.

It should be mentioned that all the results obtained in this work concern hard particle adsorption problems, when the range of interactions is much smaller than particle dimension. Such a situation can be realized experimentally for high electrolyte concentration when the electrostatic double-layer interactions are eliminated [20]. For dilute electrolytes the interaction becomes comparable with particle size that affects both adsorption kinetics and the jamming coverage. The latter parameter for interacting systems can be calculated using the effective hard particle concept developed in [20,35]. However, the range of the validity of this approximation can only be estimated by comparison with numerical simulations planned in the future.

3. Illustrative experimental results

Despite significance of particle adsorption at heterogeneous surfaces, this subject has scarcely been studied experimentally in a systematic manner. Most of early results have been obtained in indirect experiments involving packed bed columns, for hematite [50,51] and polymeric latex particles [24,52]. More systematic recent experiments have been carried out using the direct microscope observation method for polystyrene latex particles adsorbing under forced convection [40,54] or diffusion-controlled transport conditions [48,53]. As the substrate in these measurements mica surfaces precovered by smaller-sized latex particles were used. One of the studies was concerned with latex particle adsorption on mica precovered by hematite particles forming adsorption sites [54]. In this sections we shell review these works in conjunction with previous theoretical predictions.

The experiments described in Refs. [48,53,54] were carried out using the direct microscope observation method in the diffusion cell and the impinging-jet cell. Deposition kinetics and particle distribution over the substrate was followed in situ using a microscope equipped with a long-distance objective coupled with a CCD camera and an image analyzing system.

As model colloid suspensions samples of polystyrene latex were used. These latex particles of submicrometer size range are known to possess perfectly spherical shape and low polydispersity [20,35]. The negatively charged latex suspension was synthesized according to the polymerization procedure described in Ref. [55] using a persulfate initiator.

The averaged size $2a_p$ of the negative latex used in deposition experiments was 0.9 μm with standard deviation of 0.06 μm. The positively charged latex suspension (used for modelling adsorption sites) was produced and cleaned according to a similar procedure with the azonitrile initiator in place of the persulfate initiator. The averaged diameter of the positive latex $2a_s$ was 0.45 μm with the standard deviation of 0.04 μm. Hence, the particle size ratio was equal to 2 in these studies.

Zeta potential of latex samples for the ionic strength I of 10^{-3} M, adjusted by KCl addition, and pH=5.5 prevailing in these experiments was −52 mV for the negative latex and 50 mV for the positive latex, respectively.

The adsorbing (substrate) surfaces were prepared of mica sheets. Zeta potential of this mica was determined by the streaming potential method in the plane-parallel channel cell [56,57]. For the above experimental conditions zeta potential of mica was −81 mV.

The experimental procedure was the following: a freshly cleaved mica sheet was cut to the appropriate size and mounted into the diffusion cell in a vertical position or put on the top of the impinging-jet cell without using any adhesive. Then, the positive latex suspension was carefully poured into the cell. Particle deposition was carried out for a desired time (typically 15–60 min at bulk particle concentration changing in the range of 10^9–10^{10} cm^{-3}) until the prescribed surface concentration of particles was attained. The surface concentration was determined by a direct microscope counting over statistically chosen areas. The total number of particles counted was about 1000, which ensured a relative precision of coverage determination better than 3%. For sake of convenience the surface concentration of particles was expressed as the dimensionless coverage $\Theta_s=\pi a_s^2\langle N_s\rangle$ (where $\langle N_s\rangle$ is the average surface concentration of adsorbed smaller particles). After preparing the heterogeneous substrate (mica covered by adsorption sites) the positive latex suspension was replaced by 10^{-3} M KCl solution and then by the negative latex suspension and the particle deposition run was continued for a period reaching 50 h. The bulk suspension concentration of the negative latex n_b was typically 2×10^9 cm^{-3} in these experiments. Images of adsorbed particles were collected in situ at prescribed time intervals. Adsorption kinetics of latex was followed by determining the averaged surface concentration $\langle N_p\rangle$ of particles found on these images as a function of the time t. For obtaining a single point on the kinetic curve,

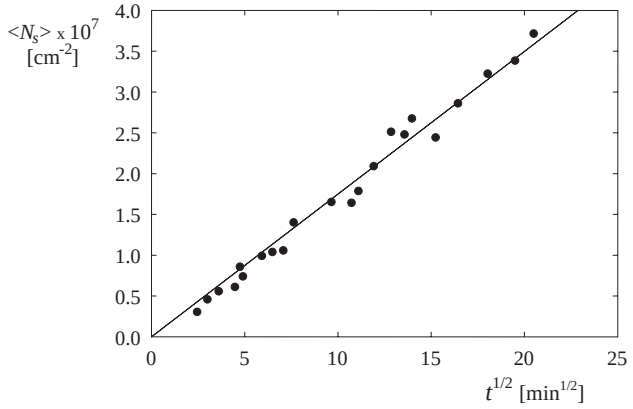

Fig. 8. Initial deposition kinetics of positive latex (average diameter 0.45 μm) at bare mica, $I=10^{-3}$ M, $n_b=2.0\times10^9$ cm^{-3} (points). The solid line denotes theoretical results calculated from Eq. (19). From Ref. [48].

500–1000 particles were counted over statistically chosen areas having typical dimensions of 100 per 100 μm. The dimensionless surface coverage of adsorbed larger particles was expressed as $\Theta_p=\pi a_p^2\langle N_p\rangle$. After completing the deposition run the latex suspension was carefully washed out by water and mica surface covered with particles was examined again under wet conditions. This procedure was selected because it has been observed that drying up of the sample induced significant structure changes in the particle monolayer.

It also was proven in these experiments [48,53,54] that particle adsorption of the positive latex on bare mica or negative latex on sites was perfectly irreversible and localized. No lateral motion or particle desorption was observed when rinsing in situ particle monolayers with electrolyte, 10^{-3} M KCl, by a prolonged period of time.

The kinetics of adsorption of positive latex (serving as adsorption sites) was quantitatively evaluated in order to select appropriate conditions for producing a desired, well-controlled surfaces coverage of sites. A typical kinetic run observed in these experiments is shown in Fig. 8. As can be seen, the surface concentration of sites $\langle N_s\rangle$ (consequently the site coverage Θ_s that is proportional to this quantity) increased linearly with the square root of the deposition time t, in accordance with diffusion-controlled transport to a plane surface, described by the formula [35,48]

$$\langle N_s\rangle = 2\sqrt{\frac{D_s t}{\pi}}n_{bs} \tag{19}$$

where $D_s=kT/6\pi\eta a_s$ is the diffusion coefficient of the particle in the bulk (k is the Boltzmann constant, T is the absolute temperature, η is the dynamic viscosity of the suspension and n_{bs} is the bulk concentration of the latex). Because both $\langle N_s\rangle$ (the averaged number of particles per unit area) and n_{bs} can be determined experimentally (the latter quantity via the direct dry weight method), one can use Eq. (19) to calculate the diffusion coefficient of particles. In this way, by knowing the temperature and the viscosity of the suspension one can determine particle size. From the kinetic run shown in Fig. 8 it was found that $2a_s=0.47$ μm, which is in a good agreement with the value obtained from the diffractometer.

Besides the coverage, the uniformity of site distributions produced according to the above procedure has been examined. First, it was demonstrated by a throughout variance analysis (carried out for various areas over the mica substrate covered by sites) that latex particle distributions were statistically uniform with no tendency to clustering as is often the case for monolayers dried before

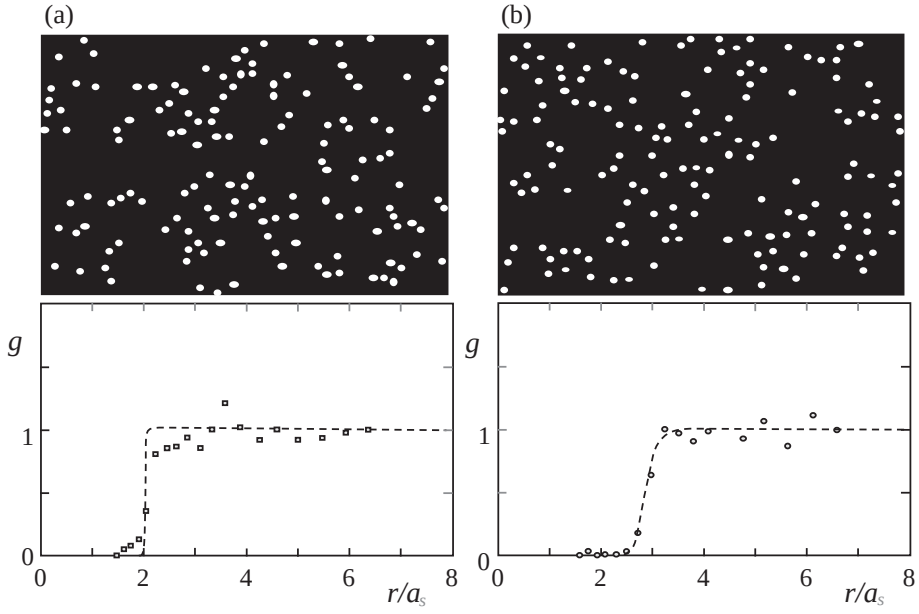

Fig. 9. Micrographs showing site distributions (positive latex particles adsorbed on mica), with the corresponding pair correlation function. (a): $\Theta_s=0.05$, $I=10^{-3}$ M; (b): $\Theta_s=0.05$, $I=10^{-5}$ M.

microscope observation. This can be seen in Fig. 9 where micrographs of sites adsorbed at mica are presented for $\Theta_s=0.05$. Quantitatively, the site distribution was analyzed in terms of the pair correlation function defined above. It can be seen that for a rather broad range of ionic strength adsorption sites were quite uniformly distributed in accordance with the Boltzmann distribution [35].

The results shown in Figs. 8 and 9 were derived for the initial stages of site deposition, when, due to their small coverage, surface blocking effects remained quite insignificant. As demonstrated in Ref. [47] such linear regimes of site deposition were observed for $\Theta_s<0.2$, depending on the ionic strength of the suspension. This can be seen in Fig. 10 presenting the kinetic runs derived using the diffusion cell. There are two interesting features of these non-linear particle deposition regimes: (i) the initial deposition rate was independent on the ionic strength being governed by the square root of time dependence; and (ii) the jamming coverage (attained after long adsorption time) increased monotonically with the ionic strength. This can be interpreted in terms of the effective interaction range concept [20,28,35] exploiting the fact that the characteristic length scale of electrostatic interactions decreases with the ionic strength. Hence, for relatively high ionic strength (10^{-2} M in our case) these interactions are effectively eliminated and particles can be treated as hard spheres. It is interesting to mention that the experimental data shown in Fig. 10 can be quantitatively interpreted by solving the governing diffusion equation with the RSA blocking function derived from Eq. (11) as the boundary condition [46,47]. By contrast the commonly used Langmuir model proved inadequate for describing surface blocking effects (dashed lines in Fig. 10).

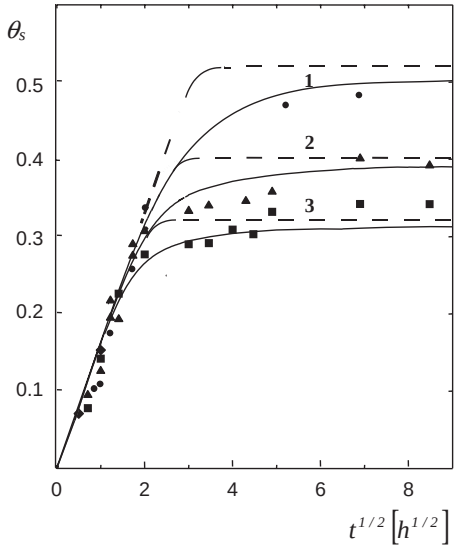

Fig. 10. Site deposition kinetics (polystyrene latex particles on mica) for the non-linear regime expressed as the dependence of Θ_s on the square root of the deposition time $t^{1/2}$. (1) $I=10^{-3}$ M; (2) $I=10^{-4}$ M; (3) $I=10^{-5}$ M. Solid lines denote the theoretical results calculated numerically by using the RSA model [46,47] and the dashed lines represent the results calculated by using the Langmuir model.

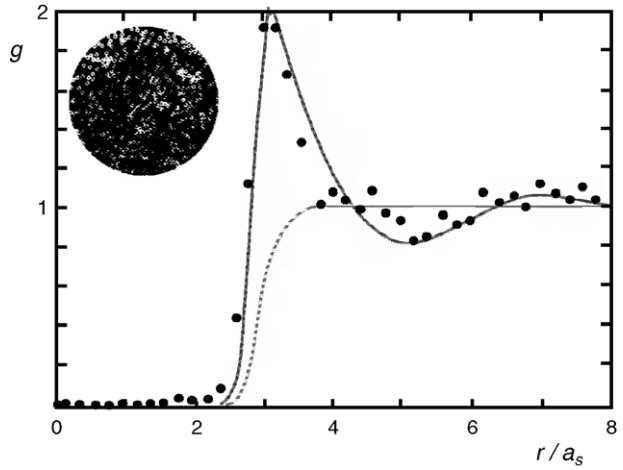

Fig. 11. The pair correlation function of sites, negative latex particles of average diameter 0.9 μm adsorbed on mica for $I=10^{-5}$ M, $\Theta_s=0.27$. The solid lines denote the theoretical pair correlation function derived from the RSA model. The dotted line denotes the Boltzmann distribution. From Ref. [20].

It is also interesting to note that for higher coverage the distribution of sites deviates significantly from the uniform distribution observed for low coverage as can be deduced from the pair correlation function shown in Fig. 11 for $\Theta_s=0.27$ and $I=10^{-5}$ M.

By exploiting these results systematic studies of larger particles deposition have been performed in Refs. [48,53,54] with the aim of determining the kinetics of particle deposition on heterogeneous surfaces as a function of site concentration Θ_s. Typical kinetic runs evaluated for initial stages of adsorption at heterogeneous surfaces when the blocking effects were negligible are shown in Fig. 12. Part (a) of this figure presents the results obtained under convection-controlled transport condition (in the impinging-jet cell) whereas in part (b) results obtained for diffusion-controlled transport are plotted. As can be noticed in Fig. 12(a) the dependence of particle coverage Θ_p on the deposition time t was linear with the slope increasing abruptly with the site coverage Θ_s (heterogeneity degree). Consequently, for Θ_s as low as a few percent, particle deposition rate at site covered surfaces attained the limiting value pertinent to uniform surfaces (these results are depicted by dashed lines in Fig. 12(a)). The linearity of the kinetic curves shown in Fig. 12(a), enables one, therefore, to determine the initial flux of particles (initial deposition rate) using the defining equation [53]:

$$|j_0| = \frac{1}{\pi a_p^2}\frac{\Delta\Theta_p}{\Delta t} \tag{20}$$

where $\Delta\Theta_p/\Delta t$ is the slope of the kinetic run fitted by a linear regression line. It also was demonstrated in separate runs that j_0 was proportional to the bulk suspension concentration n_b, indicating that particle deposition on heterogeneous surfaces was indeed a linear process. It is, therefore, advantageous to express the initial flux in the reduced form—$j_0(\Theta_s)/n_b=k_b(\Theta_s)$, where $k_b(\Theta_s)$ is the

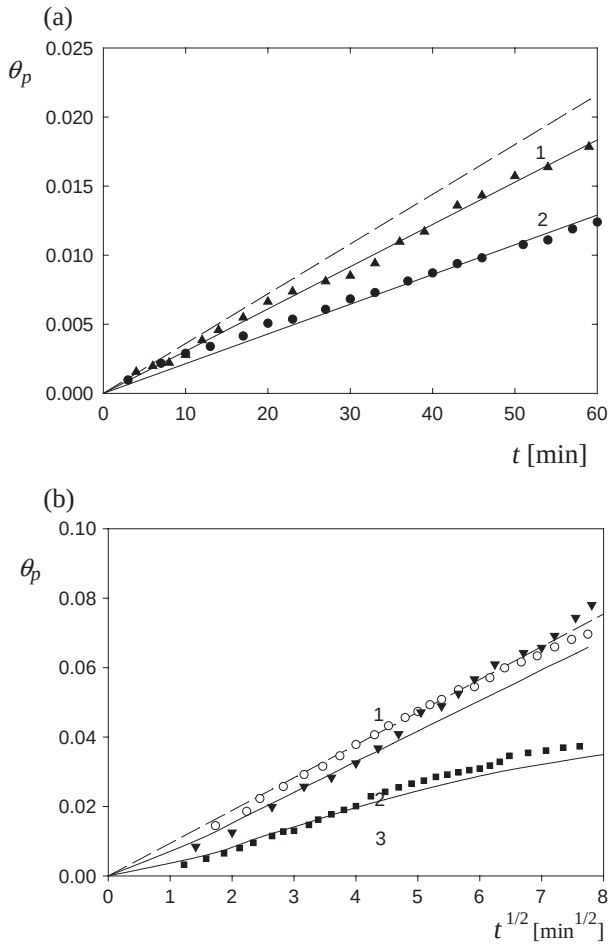

Fig. 12. Initial deposition kinetics of negative latex particles (average diameter 0.9 μm) on heterogeneous surfaces (mica covered by positive latex particles). Part (a)—the impinging-jet cell, Re=4, $n_b=1.06\times10^8$ cm^{-3}: (1) $\Theta_s=0.032$; (2) $\Theta_s=0.018$. Solid lines denote theoretical results calculated numerically by integration of Eq. (14) and the dashed line represents theoretical results predicted for homogeneous surfaces. Part (b)—the diffusion cell: (1) $\Theta_s=0.100$; (2) $\Theta_s=0.042$; (3) $\Theta_s=0.0068$. The solid lines denote theoretical results calculated numerically and the dashed line represents theoretical results predicted for homogeneous surfaces calculated from Eq. (19). From Ref. [53].

mass transfer rate constant [35,53], since averages from many runs performed for various n_b can be taken.

Analogous dependencies were observed for diffusion-controlled transport conditions (see Fig. 12(b)). In this case the initial deposition flux of particles attained the value pertinent to uniform surfaces for $\Theta_s>0.05$ and was governed by the equation [53]

$$j_{mx} = -\sqrt{\frac{D_p}{\pi t}}n_b = k_b(t)n_b \tag{21}$$

The limiting flux for uniform surfaces $j_{mx}(t)$ can be used as a useful scaling variable for expressing experimental results in the reduced form $j(\Theta_s,t)/j_{mx}(t)=k_b(\Theta_s,t)/k_b(t)$. This form of presentation of experimental results is advantageous for their theoretical analysis [53]. The dependence of the reduced flux on the site coverage Θ_s is plotted in Fig. 13. As can be observed this quantity increased abruptly approaching unity for site coverage Θ_s in the range of a few percent. These experimental evidences suggest that the initial deposition kinetics at heterogeneous surfaces can well be predicted by exploiting the well-known results pertinent to uniform surfaces [20,35]. This has a significance because many of known theoretical and experimental data for uniform surfaces can directly be transferred to heterogeneous systems.

A quantitative interpretation of the results shown in Fig. 13 can be attained in terms of the RSA model described in detail above. It was shown in Ref. [46] that the general boundary condition for the bulk transport equation of particles has the form

$$D(\delta)\left(\frac{\partial n}{\partial h}\right)_\delta = -j(\Theta_s) = k_a n_b p_0(\Theta_s) \tag{22}$$

where $D(\delta)$ is the particle diffusion coefficient at the edge of the adsorption boundary layer of the thickness δ, n is the particle number concentration at this point, $p_0(\Theta_s)$ is the initial adsorption probability of particles given by Eq. (7) and k_a is the adsorption constant that can be evaluated by straightforward integration when the particle site interaction energy is known as a function of the distance [35].

In the case of convection-controlled transport, particle flux becomes stationary after the transition time of the order of seconds [35] and Eq. (22) can be expressed in the simple analytical form

$$\frac{j(\Theta_s)}{j_{mx}} = \bar{j} = \frac{Kp_0(\Theta_s)}{1+(K-1)p_0(\Theta_s)} \tag{23}$$

where $K=k_a n_b/k_b n_b$ is the coupling constant characterising the rate of the transport through the surface boundary layer relatively to the transport in the bulk (through the diffusion

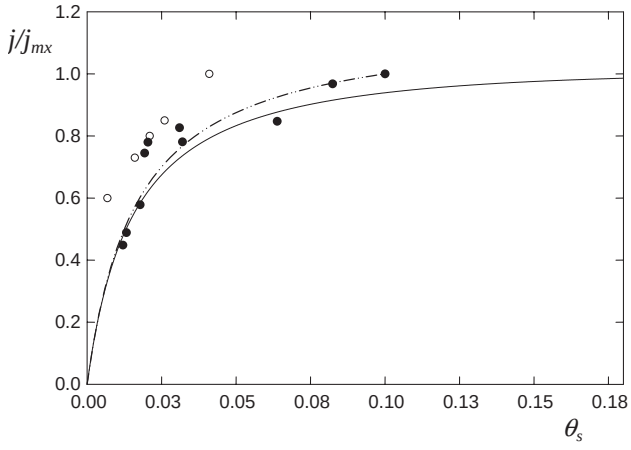

Fig. 13. The dependence of the normalized flux of particles j/j_{mx} on the site coverage Θ_s. The full points denote the experimental results obtained for the impinging-jet cell, the empty points show the results obtained for the diffusion cell, the solid line shows the theoretical results calculated from Eq. (23) and the dashed-dotted line shows the approximate analytical results calculated from Eq. (24). From Ref. [53].

layer) and $p_0(\Theta_s)$ is the initial adsorption probability given by Eq. (7).

A simple analytical expression can be derived from Eq. (23) in the case when $\lambda\Theta_s \ll 1$

$$\overline{j} = \frac{4\lambda K\Theta_s}{1+4\lambda(K-1)\Theta_s} \tag{24}$$

The theoretical results calculated from Eqs. (23) and (24) are shown in Fig. 13 (lines). As can be observed, they reflect quite well experimental results obtained for convection-controlled transport conditions. Some positive deviations of experimental data were interpreted in Ref. [53] as due to the appearance of the interception effect for higher flow intensity. It is interesting to note that the results obtained for diffusion-controlled deposition, when no simple analytical expression can be derived, are quite similar to the convection-controlled transport. In both cases the reduced flux increased abruptly with the site coverage Θ_s. This was interpreted by the fact that after a failed adsorption attempt (at the interface area devoted of sites) an adsorbing particle can reach by diffusion another accessible adsorption site in their vicinity, before it returns to the bulk of the suspension.

It should be remembered, however, that the results shown in Figs. 12 and 13 concerned initial adsorption stages when particle accumulation at the surface was not too high. Under such circumstances, the overall transport rate is governed by the diffusion transport in the bulk of the suspension rather than by the surface transport step whose rate is determined by site coverage.

The effects connected with the surface transport start to play a more significant role for high particle coverage approaching the jamming limit [47,48]. The appearance of such non-linear deposition regimes at heterogeneous surfaces can well be observed in Fig. 14. These kinetic curves were determined for Θ_s ranging from 0.016 to 0.22 and ionic strength of 10^{-3} M [48]. As can be seen, for particle coverage above 0.1 a significant deviation of adsorption kinetics from linearity (expressed in terms of the square root of adsorption time) occurred as a result of increased surface blocking effects observed previously for uniform surface adsorption (see Fig. 10). As a result, particle adsorption rate decreased gradually with the adsorption time and particle coverage attained apparent saturation values.

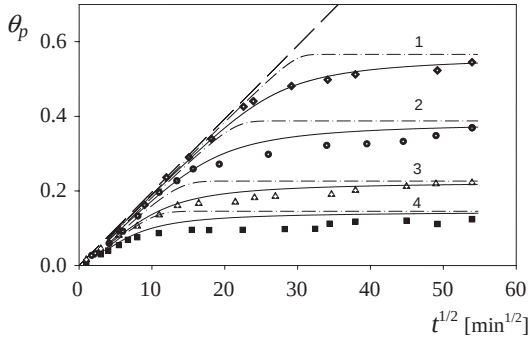

Fig. 14. Adsorption kinetics of negative latex at heterogeneous surfaces for the non-linear regime expressed as the Θ_p vs. $t^{1/2}$ dependence, $n_b = 4.8\times10^8$ cm^{-3}. (1) Θ_s=0.22, (2) Θ_s=0.06, (3) Θ_s=0.03 and (4) Θ_s=0.016. Solid lines denote the theoretical results calculated numerically by solving the diffusion equation with the RSA boundary condition; the dashed line represents the theoretical results calculated from Eq. (19) in the case of no blocking. From Ref. [48].

A quantitative interpretation of these effects can be performed analogously as for the uniform surfaces by formulating a non-linear boundary condition for the diffusion transport equation incorporating the initial adsorption probability and the available surface function [48]. Both these quantities have been determined from the Monte-Carlo simulations performed according to the above-described algorithm. The diffusion equation with this boundary condition can be solved by using the implicit finite-difference method as described in detail elsewhere [46,47]. As can be seen in Fig. 14, the experimental data obtained for various Θ_s [48] are well reflected by these theoretical calculations (depicted by solid lines) for the entire range of adsorption time studied, reaching 50 h. It is worthwhile noting that no adjustable parameters have been used by evaluating the theoretical data shown in Fig. 14 but merely the experimental value of the particle size ratio λ and the site coverage Θ_s.

It should be remembered, however, that due to the finite adsorption time the saturation values of particle coverage as shown in Fig. 14 are slightly lower than the true jamming limit. Therefore, it was suggested in Ref. [48] that the jamming coverage can be better assessed by extrapolation of the experimental data obtained for long times using the procedure proposed in Ref. [46]. The following analytical expression has been derived, whose validity was confirmed by extensive numerical calculations

$$\Theta_p^{\infty} = \Theta_1\left[1+0.372\sqrt{\frac{\Theta_1}{\xi D_p a_p n_b t_1}}\right] \tag{25}$$

where Θ_1 is the particle coverage determined experimentally for the maximum adsorption time t_1, and ξ is the dimensionless parameter of the order of 0.1 characterizing the surface transport resistance [46]. It was estimated in Ref. [48] that the correction varied between 1% and 2% for Θ_1 range shown in Fig. 14.

Other kinetic runs have been performed in Ref. [48] with the aim of obtaining the jamming coverage of particles for the entire range of site coverage. These results, both unextrapolated (empty symbols) and extrapolated (full symbols), are collected in Fig. 15. A characteristic feature of the data is that the maximum coverage of particles Θ_p is attained for site coverage as low as 0.1. This finding has profound practical implications suggesting an efficient method for detecting the presence of surface heterogeneities (nanoparticles) on surfaces by adsorption of larger colloid particles. It is also worthwhile noting that the experimental data (extrapolated) exceed for higher site coverage the limiting value of 0.547 which was predicted theoretically for homogeneous surfaces [26,29]. This is in a good agreement with the numerical simulations performed according to the

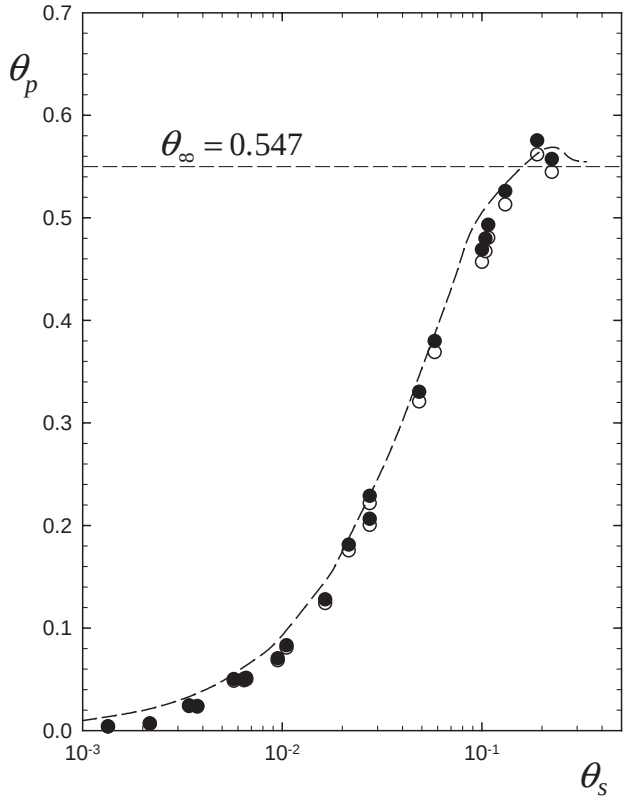

Fig. 15. The maximum (jamming) coverage of particles Θ_p^∞ as a function of site coverage Θ_s; the symbols denote experimental results obtained in the diffusion cell using latex particles, the solid line represents the theoretical Monte-Carlo simulations (smoothened) and the dashed line represents the limiting result for homogeneous surfaces. From Ref. [48].

algorithm described above (see the solid line in Fig. 15) that predicts a maximum value of Θ_p equal to 0.565 for $\Theta_s = 0.22$. A physical interpretation of the maximum is that for increasing site coverage, the surface area of sites available for particles becomes larger than the geometrical area of the interface because particles are adsorbed in different planes (quasi-3D). By increasing the site coverage, however, the average distance between sites becomes smaller than particle diameter, so a significant part of their surface area becomes inaccessible for particles. This effect is expected to reduce the available area for particles and consequently the jamming coverage.

It should be mentioned that experiments presented in Fig. 15 were carried out for the ionic strength of 10^{-3} M, so the thickness of the electric double layer was equal to 2.2% of adsorbing particle radius. As a result, the particles could not be treated as perfectly rigid spheres, which was the main assumption when performing numerical simulations. In accordance with theoretical estimations presented elsewhere [32,35] the correction to the jamming coverage stemming from electrostatic repulsion is of the order of twice the double layer thickness, i.e., 4.4% in our case. This agrees with the value found in our experiments. It is to mention that correction of this order of magnitude is not too significant from a practical viewpoint.

It is interesting to note that the good agreement of the experimental data with numerical simulations spectacularly confirmed the site multiplicity effect predicted theoretically (see Fig. 6). From numerical simulations it was predicted that for $\lambda = 2$ one site can accommodate on average 2.40 particles in the limit of low coverages of sites and particles. This value is treated as the site multiplicity factor, denoted by n_s. This result can be efficiently interpreted in terms of the geometrical model discussed previously. As mentioned, for $\lambda = 2$, at the jamming state, one site can be blocked by one, two, three or four particles. However, the one- and four-particle attachment events are highly improbable, so most of the sites bear two or three particles. Assuming equal probability of these two configurations one obtains $n_s = 2.5$, which is quite close to the theoretical and experimental values.

The multiple site coordination is expected to exert a profound effect on the distribution of particles and structure of adsorbed particle monolayer as well. This can be clearly seen in Fig. 16 where micrographs of adsorbed particles are shown for Θ_p equal to 0.04 and 0.07 in the limiting case of

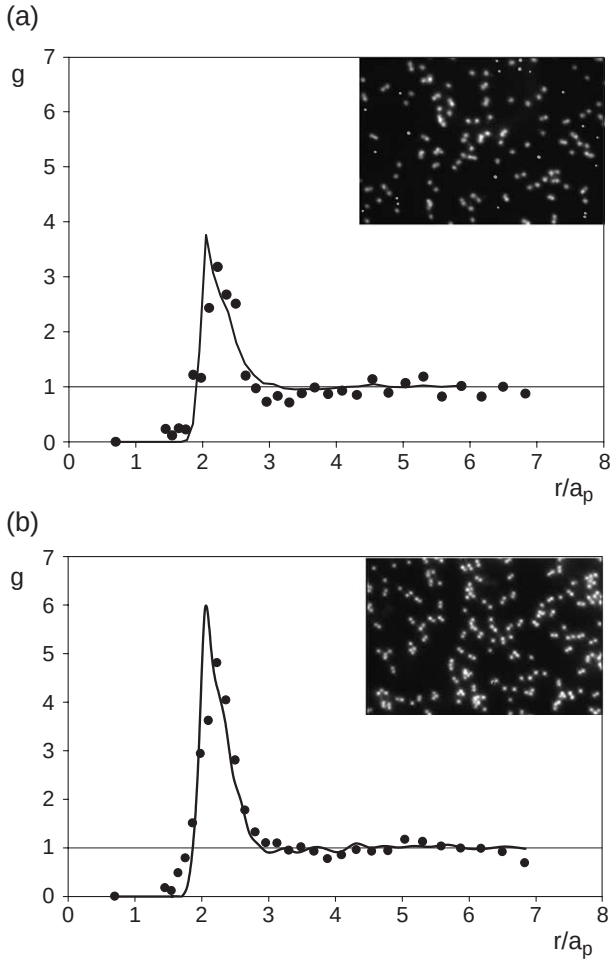

Fig. 16. Micrographs of negative latex particles (average diameter 0.9 μm) adsorbed on sites ($\Theta_s = 0.014$, $\lambda = 2$) and the corresponding pair correlation function g: part (a), $\Theta_p = 0.04$; part (b), $\Theta_p = 0.07$. The solid lines denote the theoretical pair correlation function derived from the extended RSA model. From Ref. [48].

low site coverage $\Theta_s=0.014$ [48]. As can be estimated, the average distance between sites $\sqrt{\pi a_s^2/\Theta_s}$ equals $15a_s$ for $\Theta_s=0.014$, which considerably exceeded the site and particle dimensions. This estimation indicates that the sites can be largely treated as isolated targets because particles adsorbed on various sites will not interfere with each other. This phenomenon can indeed be observed in the micrograph shown in Fig. 16 because adsorbed particles are very unevenly distributed with tendency to form assemblages, usually composed of two or three particles attached to one site. This interesting observation represents apparently the first evidence of the site multiplicity effect occurring in the colloid adsorption processes. From simple geometry one can deduce that site multiplicity effect (simultaneous attachment of more than one particle to one adsorption site) may only appear for particle to site size ratio $\lambda<4$. On the other hand, in our case, for $\lambda=2$, there could be maximum of four particles attached to one site, which qualitatively explains the appearance of particle clusters.

Due to larger particle sizes, which are visible under microscope, the distributions shown in Fig. 16 could be quantitatively evaluated in terms of the pair correlation function $g(r)$ (referred often to as the radial distribution function). The function was calculated from the constitutive dependence given by Eq. (3). A characteristic feature of the $g(r/a_p)$ function shown in Fig. 16 is that it exhibits a well-pronounced maximum at the distance $r/a_p=2$ whose height increased monotonically with particle coverage Θ_p. Another interesting fact is that this function was not vanishing for the distance $r/a_p<2$ but rather at r_{min}/a_p of about 1.7. The non-vanishing value of g observed for this distance range spectacularly confirmed the fact that particles were adsorbed in various planes as a result of the finite size of the adsorption sites. This means that their projections on the adsorption plane could overlap. This apparent overlapping effect is analogous to previously observed for adsorption at homogeneous interfaces of polydisperse particles [30]. It is interesting to compare the experimentally found minimum distance r_{min} with the value predicted theoretically for particle size ratio occurring in our experiments. This can be done by realizing that the minimum distance between projections of particle centers appears when one particle touches the substrate surface and simultaneously another particle (and obviously the site). Moreover, the centers of the two particles and the site lie in one plane perpendicular to the substrate surface. From a simple geometry one can deduce then that the distance r_{min} is given by the expression

$$r_{min}/a_p=2\left[2a_p\sqrt{a_pa_s}+(a_p-a_s)\sqrt{a_s(2a_p+a_s)}\right]/(a_p+a_s)^2 = 2[2\lambda\sqrt{\lambda}+(\lambda-1)\sqrt{2\lambda+1}]/(1+\lambda)^2 \quad (26)$$

where, as mentioned above, $\lambda=a_p/a_s$.

One can predict from Eq. (26) that for our geometry, when $\lambda=2$, $r_{min}/a_p=1.75$ that agrees well with the value found experimentally (see Fig. 16). Interestingly enough, one can calculate from Eq. (26) that for $\lambda=4$, $r_{min}/a_p=2$, which agrees with previous conclusion that $\lambda=4$ is the limiting value when two particles can be attached to one site.

On the other hand, from geometrical considerations one also can predict the maximum distance r_{mx} between two particles attached to one site and contacting simultaneously the substrate surface. It is given by the simple formula (valid for $\lambda<4$)

$$r_{mx}/a_p=4/\sqrt{\lambda} \quad (27)$$

As can be deduced, in our case $r_{mx}/a_p=4/\sqrt{2}=2.83$. One can expect that for distances larger than r_{mx} the pair correlation function g should approach unity since adsorbed particle positions remain uncorrelated (particles adsorbed on various sites do not interfere with each other as mentioned above). Indeed, one can observe in Fig. 16 that g approaches unity for $r/a_p>2.8$.

It is interesting to observe that all the characteristic features of the correlation function shown in Fig. 16 are well reflected by theoretical predictions depicted by solid lines. These theoretical results have been derived from Monte-Carlo simulations performed according to the model discussed above.

A good agreement of experimental and simulation data with the analytical estimations derived from Eqs. (26) and (27) indicates that by analyzing the shape of the pair correlation function (especially the r_{min} and r_{mx} values) important clues can be gained about the size and coverage of sites present at a substrate. Obviously, this possibility is especially attractive for sites of unknown size, invisible under optical microscope.

In Fig. 17 analogous results obtained recently [58] for $\lambda=1$ (equal particle and site ratio) are presented. As can be noticed in the micrograph showing adsorbed particles at $\Theta_s=0.015$ and $\Theta_p=0.06$ ($I=10^{-3}$ M) a significant tendency to clustering is observed. The surface aggregates are

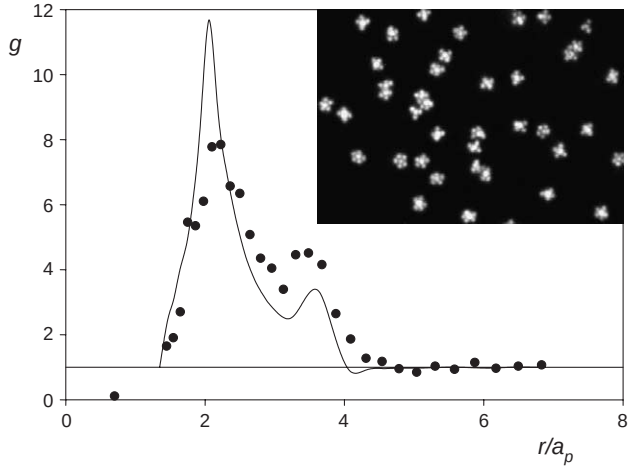

Fig. 17. Micrographs of negative latex particles (average diameter 0.9 μm) adsorbed on sites ($\Theta_p=0.06$, $\Theta_s=0.015$, $\lambda=1$) and the corresponding pair correlation function g. The solid lines denote the theoretical pair correlation function derived from the extended RSA model. From Ref. [58].

mainly composed of four and five particles coordinated around one site (the averaged coordination number n_s was equal to 4 for these experimental conditions). This confirms again the hypothesis that particle clusters of targeted composition can be produced by exploiting the above procedure. Formation of surface clusters is evidently expressed in the pair correlation function shown in Fig. 17. A large primary maximum (peak) is observed at r_p equal to approximately 2, i.e., when two adsorbing particles are almost in contact. There also appears a minimum and a secondary maximum at $r_p = 3.5$. It is interesting to note that all these peculiar features of experimentally determined pair correlation function are in a full agreement with theoretical simulations (solid line in Fig. 17) performed according to the above RSA model. Accordingly, the minimum and maximum distances r_{min} and r_{mx} calculated from Eqs. (26) and (27) agree well with experimentally found values, i.e., 1 and 4, respectively.

Although all above discussed results have been obtained for model colloid systems they can be used as useful reference systems for analyzing more interesting practical situations, e.g., polyelectrolyte adsorption, exploited widely for producing multilayered particle coatings [9–13]. Interesting experiments of this kind have recently been performed by Serizawa et al. [3,4] who deposited negatively charges polystyrene latex particles on polyelectrolyte films produced by consecutive adsorption of poly(allylamine hydrochloride) (PAH) and poly(sodium 4-styrenesulfonate) (PSS). The indirect quartz crystal microbalance technique (QCM) was used to evaluate the amount of deposited latex particles. It was proven that particle adsorption was strictly correlated with the charge of the outermost polyelectrolyte layer: deposition was significant on PAH terminated multilayer, whereas it was practically negligible for PSS terminated multilayer. However, because of the limited accuracy of the QCM technique no further quantitative analysis was performed.

More elaborated experiments of this type have been reported in Ref. [59]. Consecutive multilayers of PAH and PSS (both of a molecular weight of ca. 70,000) have been produced on mica from polyelelectrolyte concentration of 500 ppm at pH = 7.4 and the ionic strength of 10^{-3} M. It was predicted [60,61] that under this adsorption conditions the consecutive polyelectrolyte multilayers did not show too extensive interpenetration because the chains were adsorbing side-on due to electrostatic attraction. On the other hand, the electrostatic repulsion between chains of the same polyelectrolyte lead to a rather loose structure of each layer (coverage of the range of 0.3 was estimated) resembling closely the particle monolayers analyzed above. Positively charged polystyrene latex particles (having averaged diameter of 0.45 μm and zeta potential of 69 mV) were then deposited on multilayers terminated with PAH and PSS. The direct microscope observation technique was again used to enumerate the quantity of deposited particles. The results shown in Fig. 18 unequivocally demonstrated that particle

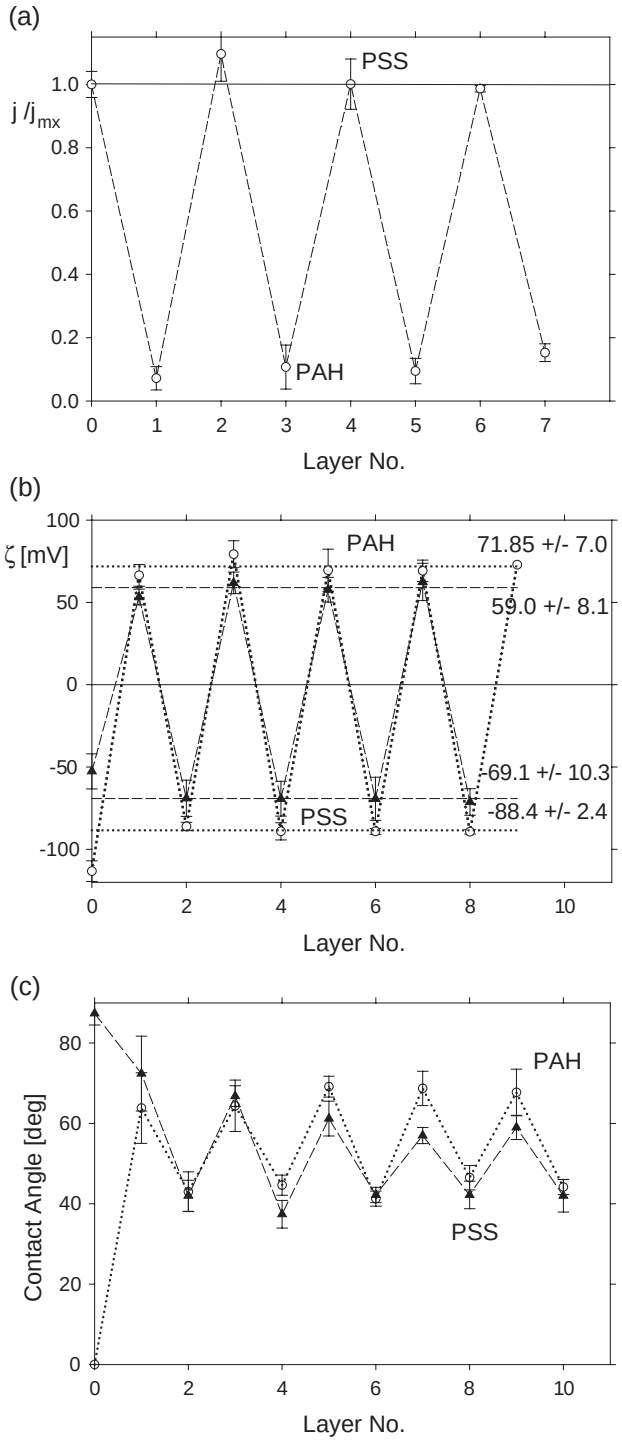

Fig. 18. Oscillatory variations in the latex particle deposition rate observed for mica covered by polyelectrolyte multilayers (consecutively PAH and PSS)—part (a), same variations in substrate zeta potential determined by the streaming potential method—part (b), and in the dynamic contact angle—part (c). From Ref. [59].

deposition was strictly correlated with the charge of the outermost layer, i.e., there was practically negligible deposition of particles on PAH layers and deposition with maximal initial rate on PSS layers. In contrast to the results of Serizawa et al. [3,4], however, the results presented in

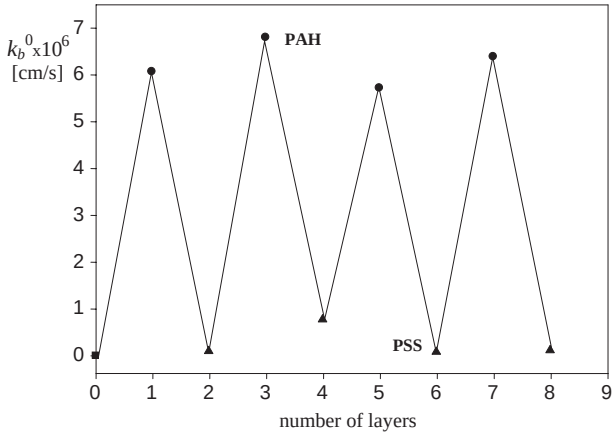

Fig. 19. Oscillatory variations in the particle deposition rate observed for modified titanium covered by polyelectrolyte multilayers (consecutively PAH and PSS).

Ref. [59] could be quantitatively interpreted because particle deposition rate (initial flux) was measured directly. It was found that the measured flux in the case of the PSS layer was identical within the experimental error with the maximum flux characteristic for uniform surfaces. Additionally, both were in a quantitative agreement with theoretical predictions stemming from the convective diffusion theory. Hence, the results shown in Fig. 18 are consistent with those previously discussed for the particle/site system. This confirms the hypothesis of a negligible interpenetration of polymeric chains between consecutive layers.

It is interesting to observe that the oscillatory changes in the particle flux shown in Fig. 18 are strictly correlated with oscillations in the zeta potential of multilayers (measured by using the streaming potential method [56,57]) and periodic variations in the contact angle of water drops on dried multilayers [61].

The same tendency was observed for the more practically relevant case of polyelectolyte multilayer adsorption on titanium surfaces oxidized electrochemically in order to produce a titania layer of controlled thickness [61]. Similarly as above, consecutive multilayers of PAH and PSS and then negative latex particles (0.66 μm in diameter) have been deposited. The results plotted in Fig. 19 show similar oscillations in particle flux between the maximum value (for PAH terminated multilayer) and practically negligible values for the PSS terminated multilayer.

The same technique of colloid imaging can be used qualitatively to visualize in a fast and efficient manner various polymeric structures produced in polyelectrolyte multilayer deposition. One of such spectacular examples is shown in the set of micrographs in Fig. 20. These structures have been produced by deposition of PSS layer on poly(ethylene imine) (PEI) of a molecular weight of 750,000 under flowing conditions.

From the results shown in Figs. 18–20 one can conclude, therefore, that colloid particles can be used as sensitive detectors of the presence of nanometric features at various solid substrates.

4. Conclusions

It was demonstrated that initial adsorption rate of particles at heterogeneous surfaces covered by spherical adsorption sites increases rapidly with site coverage, which

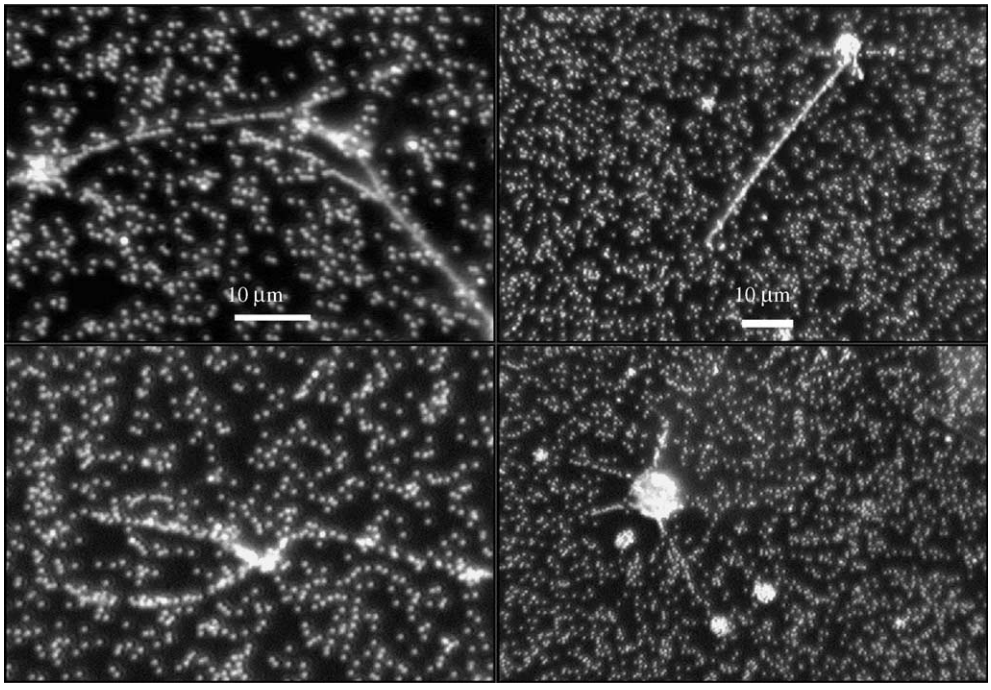

Fig. 20. Polymeric structures detected by adsorbing colloid particles.

is in agreement with theoretical predictions derived for RSA simulations, approximated by analytical expression, Eq. (23). It was found that for site coverage $\Theta_s > 1/4\lambda$ (being practically of the order of a few percent) the rate of particle deposition attains the maximum value characteristic to homogeneous surfaces. This was attributed to the fact that the overall transport was controlled by bulk diffusion of particles rather than by the surface transport resistance.

For higher coverage of particles adsorption kinetics deviated from linearity because of the appearance of blocking effects. This effect was quantitatively accounted for by the theoretical approach based on numerical solutions of the diffusion equation with the non-linear boundary conditions derived from RSA simulations. The extrapolation of the kinetic runs allowed one to determine accurately the jamming coverage Θ_p as a function of the site coverage Θ_s. The experimental data were found in a good agreement with numerical simulations confirming a rapid increase in the jamming coverage of particles with site coverage and the presence of a maximum on the Θ_p vs. Θ_s curve. These findings have been explained in terms of the multiple site coordination and quasi-3D adsorption of particles. It also was shown that these effects influenced significantly structure of particle monolayers characterized in terms of the pair correlation function. Based on these experimental evidences it was suggested that colloid particle deposition on heterogeneous surface covered by sites can be exploited as an efficient method for producing surface clusters of a targeted architecture.

It also was demonstrated that controlled adsorption of colloid particles on sites of nanometric scale can be exploited for a direct visualization of surface features, e.g., polyelectrolyte chains attached to solid surfaces.

Acknowledgments

This work was supported by the KBN Grant 4T09A 076 25 and partially by the EC Grant GRD1-2000-26823.

References

[1] Boluk MY, van de Ven TGM. Colloids Surf 1990;46:157.
[2] Lvov Y, Ariga K, Ichinose I, Kunitake T. J Am Chem Soc 1995;117:6120.
[3] Serizawa T, Takashita H, Akashi M. Langmuir 1998;14:4088.
[4] Serizawa T, Kamimura S, Akashi M. Colloids Surf 2000;164:237.
[5] Fulda K-U, Piecha D, Ticke B, Yarmohamdipour H. Prog Colloid Polym Sci 1996;101:178.
[6] Schmitt J, Machtle P, Eck D, Mohwald H, Helm CA. Langmuir 1999;15:3256.
[7] Chen KM, Jiang X, Kimmerling LC, Hammond PT. Langmuir 2000;16:7825.
[8] Ngankam AP, Mao G, Van Tassel PR. Langmuir 2004;20:3362.
[9] Lvov Y, Ariga K, Onda M, Ichinose I, Kunitake T. Langmuir 1997;13:6195.
[10] Jiang C, Markutsya S, Tsukruk VV. Langmuir 2004;20:882.
[11] Sun CY, Hao E, Zhang X, Yang B, Gao M, Shen J, et al. Langmuir 1997;13:5168.
[12] Schmitt J, Decher G, Geer RE, Dressick WJ, Calvert JM. Adv Mater 1997;9:61.
[13] Kotov NA, Dekany I, Fendler JH. J Phys Chem 1995;99:13065.
[14] Chase HA. Chem Eng Sci 1984;39:1099.
[15] Willner I, Lion-Dagan M, Marx-Tibbon S, Katz E. J Am Chem Soc 1995;117:6581.
[16] Katz E, Buckmann AE, Willner I. J Am Chem Soc 2001;123:10752.
[17] Inerowicz HD, Howell S, Reniger FE, Reifenberger R. Langmuir 2002;18:2563.
[18] Howell SW, Inerowicz HD, Reifenberger R. Langmuir 2003;19:436.
[19] Adamczyk Z, Zembala M, Siwek B, Czarnecki J. J Colloid Interface Sci 1986;110:188.
[20] Adamczyk Z, Siwek B, Zembala M, Belouschek P. Adv Colloid Interface Sci 1994;48:151.
[21] Rudziński W, Charmas R, Partyka S, Thomas F, Bottero JY. Langmuir 1992;8:1154.
[22] Elimelech M, O'Melia CR. Langmuir 1990;6:1153.
[23] Song L, Elimelech M. J Colloid Interface Sci 1994;167:301.
[24] Johnson PR, Sun N, Elimelech M. Environ Sci Technol 1996;30:3284.
[25] Widom B. J Chem Phys 1966;44:3888.
[26] Hinrichsen EL, Feder J, Jossang T. J Stat Phys 1986;44:793.
[27] Schaaf P, Talbot J. J Chem Phys 1989;91:4401.
[28] Adamczyk Z, Siwek B, Zembala M, Weroński P. J Colloid Interface Sci 1990;140:123.
[29] Evans JW. Rev Modern Phys 1993;65:1281.
[30] Adamczyk Z, Siwek B, Zembala M, Weroński P. J Colloid Interface Sci 1997;185:236.
[31] Adamczyk Z, Senger B, Voegel JC, Schaaf P. J Chem Phys 1999;110:3118.
[32] Adamczyk Z, Weroński P. Adv Colloid Interface Sci 1999;83:137.
[33] Senger B, Voegel JC, Schaaf P. Colloids Surf A Physicochem Eng Asp 2000;165:255.
[34] Senger B, Schaaf P, Voegel JC, Johner A, Schmitt A, Talbot J. J Chem Phys 2000;97:3813.
[35] Adamczyk Z. In: Toth J, editor. Adsorption: theory, modeling and analysis. New York: Marcel-Dekker; 2002. p. 251–374 Chapter 5.
[36] Jin X, Wang NHL, Tarjus G, Talbot J. J Phys Chem 1993;97:4256.
[37] Jin X, Talbot J, Wang NHL. AIChE J 1994;40:1685.
[38] Adamczyk Z, Weroński P, Musiał E. J Chem Phys 2002;116:4665.
[39] Adamczyk Z, Weroński P, Musiał E. J Colloid Interface Sci 2002;248:67.
[40] Adamczyk Z, Siwek B, Weroński P, Musiał E. Appl Surf Sci 2002;196:250.
[41] Adamczyk Z, Weroński P. J Chem Phys 1998;108:9851.
[42] Adamczyk Z, Weroński P, Musiał E. J Colloid Interface Sci 2001;241:63.
[43] Senger B, Schaaf P, Voegel J-C, Johner A, Schmitt A, Talbot J. J Chem Phys 1992;97:3813.
[44] Wojtaszczyk P, Bonet Avalos J, Rubi JM. Europhys Lett 1997;40:299.
[45] Faraudo J, Bafaluy J. J Chem Phys 2000;112:2003.
[46] Adamczyk Z. J Colloid Interface Sci 2000;229:477.
[47] Adamczyk Z, Szyk L. Langmuir 2000;16:5730.
[48] Adamczyk Z, Jaszczółt K, Siwek B, Weroński P. J Chem Phys 2004;120:1155.
[49] Reiss H, Frisch HL, Lebowitz JL. J Chem Phys 1959;31:369.
[50] Ryde N, Kihara H, Matijevic E. J Colloid Interface Sci 1992;151:421.
[51] Zelenev A, Privman V, Matijevic E. Colloids Surf A Physicochem Eng Asp 1998;135:1.
[52] Johnson PE, Sun N, Elimelech M. Langmuir 1995;11:801.
[53] Adamczyk Z, Siwek B, Weroński P, Jaszczółt K. Colloids Surf A Physicochem Eng Asp 2003;222:15.
[54] Adamczyk Z, Siwek B, Musiał E. Colloids Surf A Physicochem Eng Asp 2003;214:219.
[55] Goodwin JW, Hearn J, Ho CC, Ottewill RH. Colloid Polym Sci 1974;252:464.

[56] Zembala M, Adamczyk Z. Langmuir 2000;16:1593.
[57] Zembala M, Adamczyk Z, Warszyński P. Colloids Surf A Physicochem Eng Asp 2003;222:329.
[58] Jaszczółt K, Adamczyk Z, Weroński P. Langmuir, submitted.
[59] Michna A, Adamczyk Z, Zembala M. Colloids Surf. A in press.
[60] Adamczyk Z, Zembala M, Warszyński P, Jachimska B. Langmuir 2004;20:10517.
[61] Zembala M, Adamczyk Z,Warszyński P, Kolasińska M. Colloids Surf A Physicochem Eng Asp; 2005 [in press].